Prognostic PET ^{18}F-FDG Uptake Imaging Features Are Associated with Major Oncogenomic Alterations in Patients with Resected Non–Small Cell Lung Cancer

Viswam S. Nair[1], Olivier Gevaert[4], Guido Davidzon[3], Sandy Napel[4], Edward E. Graves[5], Chuong D. Hoang[2,6], Joseph B. Shrager[2,6], Andrew Quon[3], Daniel L. Rubin[4], and Sylvia K. Plevritis[4]

Abstract

Although 2[18F]fluoro-2-deoxy-D-glucose (FDG) uptake during positron emission tomography (PET) predicts post-surgical outcome in patients with non–small cell lung cancer (NSCLC), the biologic basis for this observation is not fully understood. Here, we analyzed 25 tumors from patients with NSCLCs to identify tumor PET-FDG uptake features associated with gene expression signatures and survival. Fourteen quantitative PET imaging features describing FDG uptake were correlated with gene expression for single genes and coexpressed gene clusters (metagenes). For each FDG uptake feature, an associated metagene signature was derived, and a prognostic model was identified in an external cohort and then tested in a validation cohort of patients with NSCLC. Four of eight single genes associated with FDG uptake (*LY6E*, *RNF149*, *MCM6*, and *FAP*) were also associated with survival. The most prognostic metagene signature was associated with a multivariate FDG uptake feature [maximum standard uptake value (SUV_{max}), $SUV_{variance}$, and SUV_{PCA2}], each highly associated with survival in the external [HR, 5.87; confidence interval (CI), 2.49–13.8] and validation (HR, 6.12; CI, 1.08–34.8) cohorts, respectively. Cell-cycle, proliferation, death, and self-recognition pathways were altered in this radiogenomic profile. Together, our findings suggest that leveraging tumor genomics with an expanded collection of PET-FDG imaging features may enhance our understanding of FDG uptake as an imaging biomarker beyond its association with glycolysis. *Cancer Res; 72(15); 3725–34. ©2012 AACR.*

Introduction

Non–small cell lung cancer (NSCLC) remains the number one cause of cancer-related mortality for men and women in the United States, and its prevalence continues to increase worldwide (1). Despite potentially curative resection in early-stage NSCLCs, survival remains suboptimal and recurrence rates are high (2).

2[18F]Fluoro-2-deoxy-D-glucose (FDG) positron emission tomographic (PET) imaging is currently the standard of care for preoperative staging of disease in NSCLC, and multiple investigations suggest that the intensity of FDG uptake in the tumor before surgery is a useful biomarker for tumor aggressiveness and patient outcome postoperatively (3–5). This is an important finding as PET imaging is noninvasive, cost-effective, and routinely conducted for patients preoperatively (6–9).

PET-FDG uptake is governed by GLUT transporter uptake and metabolized to an inert intracellular product by a key regulatory enzyme in glycolysis, hexokinase-2 (HK2; ref. 10). The biologic basis for the use of FDG as a biomarker is not fully understood, but upregulated glycolysis that results in increased FDG uptake has been associated with tumor growth, metastasis, and immune evasion (11–14). Recently, a key driver that seemingly promotes a less favorable cellular energy profile was discovered [pyruvate kinase isoenzyme M2 (PKM2); ref. 15–17] and has been implicated with other major genes involved in oncogenesis that may help to explain a mechanistic switch to a glycolytic phenotype (18).

To date, no studies have examined differential genome-wide expression across varying FDG uptake levels in NSCLCs. We explored this relationship in a cohort of patients with NSCLCs to identify individual genes and gene expression signatures associated with prognostically relevant FDG uptake features.

Patients and Methods

Study design

We used a novel biocomputational approach to associate gene expression with prognostic FDG uptake features (Fig. 1) using 3 cohorts (study, external, and validation cohorts). Use of all 3 cohorts allowed us: (i) to associate FDG uptake features to gene expression, (ii) to generate a model of image features in

Authors' Affiliations: Divisions of [1]Pulmonary & Critical Care Medicine, [2]Thoracic Surgery, and [3]Nuclear Medicine, Departments of [4]Radiology and [5]Radiation Oncology, Stanford University School of Medicine, Stanford; and [6]Veterans Administration Palo Alto Health Care System, Palo Alto, California

V.S. Nair and O. Gevaert contributed equally to this work.

Corresponding Author: Sylvia K. Plevritis, Department of Radiology, Stanford University School of Medicine, Stanford, CA 94305. Phone: 650-725-4936; Fax: 650-723-5795; E-mail: sylvia.plevritis@stanford.edu
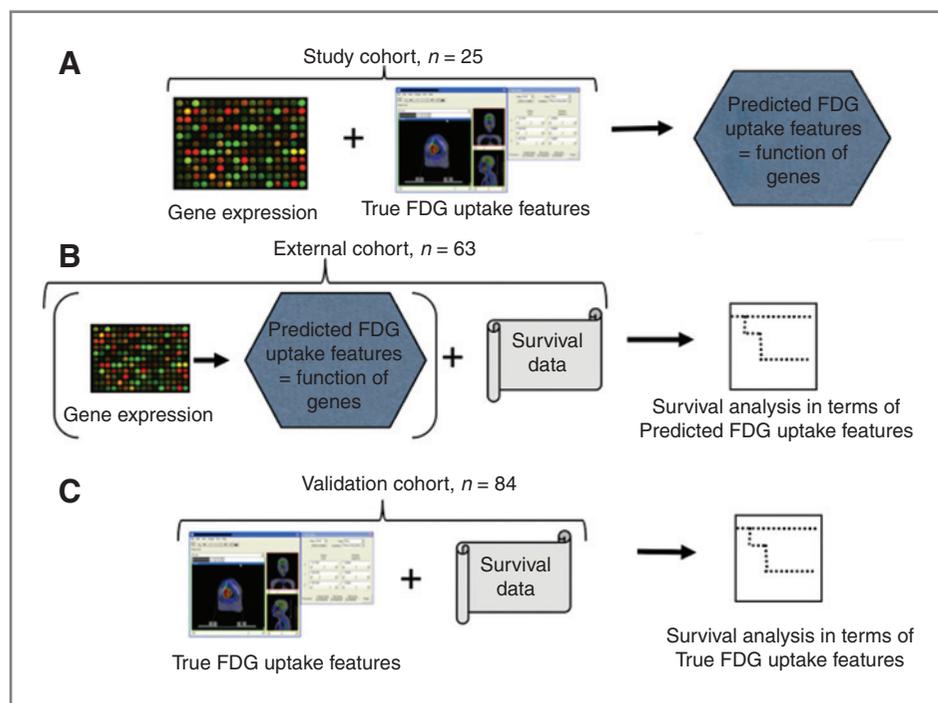
Figure 1. Study design. A, twenty-five patients with NSCLC and PET imaging before resection had genome-wide expression conducted on cryopreserved tissues (study cohort). FDG uptake features were extracted and predicted in terms of a gene signature. B, predicted FDG uptake features (prefixed by "*p*" in this study) were examined in a second (external) cohort with NSCLC outcome data and gene expression. C, validation of the predicted FDG uptake features that were identified as prognostic in the external cohort was conducted in a third (validation) cohort with PET imaging and outcome data to determine whether the true FDG uptake features remained significantly associated with overall survival.

terms of their gene expression (study cohort), (iii) to identify prognostic gene signatures from this model (external cohort), and finally (iv) to examine whether image features associated with prognostic gene sets were predictive of clinical outcome (validation cohort). To build prognostic gene expression signatures associated with FDG uptake image features, we applied our previously described radiogenomics strategy (19).

Study, external, and validation cohorts

For the study cohort, a group of patients with surgically resected NSCLC between 2008 and 2010 from 2 medical centers were retrospectively identified. All patients had pre-operative PET/computed tomographic (CT) scans analyzed for tumor FDG uptake features matched with excised tumor specimens subjected to global gene expression analysis. Patients receiving neoadjuvant therapy were excluded, and follow-up data were not available for the study cohort, as these cases were taken from recent operative specimens. For the external cohort, we used data from a previous study that modeled gene expression and outcome in patients with NSCLCs (GSE8894; ref. 20). For the validation cohort, we examined patients with resected, limited stage NSCLCs from 2003 to 2010 who underwent treatment-naive, preoperative PET imaging. Death was assessed using the National Death Index (www.cdc.gov/nchs/ndi.htm), and patients not dead were assumed to be alive at the time of data extraction (June 2011). All work was conducted with the Institutional Review Board authorization of both participating centers.

PET acquisition and FDG uptake feature extraction in study and validation cohorts

PET/CT images were acquired using either an LS PET/CT (slice thickness, 3–5 mm) at Stanford or GE Discovery VCT (slice thickness, 3.75 mm) at the Veterans Administration Palo Alto Health Care System (VAPAHCS). At Stanford, patients fasted for a minimum of 8 hours, a dose of 12 to 17 millicuries (mCi) of FDG was administered, and patients were scanned from the skull base to mid-thigh using multiple bed positions every 5 minutes approximately 45 to 60 minutes after injection. Before injection of FDG, patients who had a blood glucose level of >180 mg/dL were excluded. At the VAPAHCS, patients fasting for 6 hours had FDG injected to a target of 15 mCi at time of scan, which ranged from 60 to 120 minutes after injection and those patients who had a blood glucose of level of >200 mg/dL were rescheduled. Patients were scanned from skull to mid-thigh using multiple bed positions every 2 to 3 minutes. CT-attenuated data were reconstructed using ordered subset expectation maximization for both scanner sites.

FDG uptake was quantified using the maximum standard uptake value (SUV_{max}) by a certified nuclear medicine physician (A. Quon). The region of interest (ROI) for each nodule was drawn using the trans-axial image that was thought to represent the most FDG-avid portion around the entire lesion, and the maximum SUV pixel within the ROI (SUV_{max}) was recorded. Partial volume correction was not used for this interpretation. All DICOM images for both study and validation cohorts were then imported into an imaging feature extraction program, RT_Image (http://rtimage.sourceforge.net). FDG uptake metrics were calculated after co-registration with CT images of the tumor and then by defining an automated ROI on the PET image using a region-growing algorithm bounded by a standard threshold uptake above background, with a lower bound set at 50% of the maximum value within the ROI (21).

Fourteen metrics of interest related to SUV were recorded: SUV minimum, maximum, mean, median and percentile (75

and 90) features were extracted to define the intensity of FDG uptake in tumor; SUV standard deviation, variance, skew, and kurtosis features were extracted to measure the variation in FDG uptake across the tumor; and metabolic tumor volume (MTV), registration points (number of voxels used to define the MTV), area and total glycolytic volume (TGV) quantified the spatial extent of FDG uptake. TGV is represented in this study as the product of SUV_{mean} and metabolic volume and represents the "integrated" metabolic uptake across the tumor (22).

Comparison of study and validation cohorts

Basic descriptive clinical, pathologic, and imaging characteristics were tabulated for study and validation cohorts. Continuous variables with median and interquartile range or categorical variables with percentage were calculated. Differences between the study and validation cohorts were assessed using the Student t test for continuous variables or a χ^2 or Fisher exact test (for <5 data points in a level) for categorical variables.

Gene expression microarray data

Tumors from the study cohort were processed from a 3 to 5 mm cross-section after removal of fibrotic or necrotic areas during surgical excision (C.D. Hoang and J.B. Shrager). Tumor tissue was snap-frozen within 30 minutes and extracted to RNA using standard commercial kits. Genome-wide arrays were processed by the Stanford Functional Genomics Facility using Illumina Whole Genome Bead Chips (Human HT-12). Microarray data were filtered on the basis of a significant detection call in at least 60% of the samples and log-transformed using quantile normalization to account for array variation. Microarray data were submitted to Gene Expression Omnibus (GEO) under accession number GSE28827.

Statistical analysis

Basic descriptive clinical, pathologic, and imaging characteristics were tabulated for study and validation cohorts. Continuous variables with median and interquartile range or categorical variables with percentage were calculated. Differences between the study and validation cohorts were assessed using the Student's t test for continuous variables or a χ^2 or Fisher exact test (for <5 data points in a level) for categorical variables.

Association of FDG uptake features and gene expression

Basic correlations among FDG uptake features and for FDG uptake features with gene expression were conducted using a Spearman rank correlation test. Significance analysis of microarrays (SAM) was conducted to define genes significantly associated with FDG uptake metrics. Because of the potential for false-positive associations due to multiple comparisons, we used the false discovery rate (FDR; $q < 0.05$) to assess statistical significance (23). In addition, because single gene associations with image features are more prone to noise, a clustering method to reduce the dimensionality of the microarray data was used in addition to univariate SAM analysis (19). We clustered the microarray data using an iterative k-means clustering algorithm with 200 iterations and a coherence of

0.75; these settings were determined such that the average cluster homogeneity in external data sets was maximal (20, 24), where cluster homogeneity was defined as the average correlation between each member of the cluster within the cluster centroid. This clustering algorithm resulted in 102 clusters that were then filtered on the basis of a homogeneity of at least 0.30 in 1 of 2 external data sets (19, 24), to yield 56 high-quality clusters, defined in this study as metagenes, for further analysis (19).

Principal components analysis of FDG uptake features

We examined the principal components defining FDG uptake for the 14 features extracted to determine which features accounted for most of the variability of FDG uptake. Each principal component was defined as a linear combination of the 14 original features and could be interpreted on the basis of the weights associated with each of these features. We restricted our analysis to the first three principal components and incorporated these new features to the study cohort data set for further analyses.

Predicted FDG uptake features and their association with overall survival

Individual genes associated with FDG uptake in the study cohort were directly analyzed in the external cohort for their association to clinical outcomes. In addition, a multivariate model of FDG uptake features in the study cohort for each of the 14 features studied was built by a linear combination of metagenes to further examine the likely underlying biology of the features and their association with outcome in the external cohort. The accuracy of gene signatures to predict FDG uptake features was determined by examining the absolute difference in the predicted FDG uptake feature with the actual imaging feature value (19). Only signatures with an accuracy of greater than 0.70 were carried forward for further analysis and analyzed with outcome in the external data set. We refer to these features, now defined in terms of a gene signature, as "predicted FDG uptake features" and denote them with a prefix "p" (i.e., $pSUV_{max}$ represents the prognostic gene signature associated with SUV_{max}). Kaplan–Meier curves were dichotomized at the median gene expression value, and unadjusted Cox proportional hazards (CPH) testing was conducted to assess the prognostic significance–predicted FDG uptake features and individual genes that were highly correlated to FDG features. We also conducted Lasso CPH modeling (25) with 10-fold cross-validation to identify a multivariate signature of multiple predicted FDG uptake features whose gene expression signature was associated with outcome, creating the "multivariate-SUV" model.

Validation of prognostic FDG uptake features

We studied FDG uptake features associated with prognostic gene signatures (i.e., pFDG features) from the external cohort in a validation cohort that consisted of 84 patients with PET imaging and survival data. We analyzed extracted FDG uptake features, computed their principal components, and derived the multivariate-SUV model by Lasso CPH analysis. To describe outcomes for these features, Kaplan–Meier curves

were dichotomized at the median FDG uptake feature value and unadjusted CPH testing was conducted. Finally, we analyzed the prognostic significance of age, tumor size, and stage for the external and validation cohorts separately, followed by multivariate analyses with univariately derived prognostic imaging features to determine whether these imaging features added statistically significant independent information to prognosis in both cohorts.

Gene enrichment analysis of predicted FDG uptake features

We used a hypergeometric test with multiple testing correction and FDR (26) for metagene enrichment analysis using gene set collections from GeneSigDb (http://compbio.dfci.harvard.edu/genesigdb/), the NIH Database for Annotation, Visualization and Integrated Discovery (DAVID; http://david.abcc.ncifcrf.gov; ref. 27), MSigDb (http://www.broadinstitute.org/gsea/msigdb/index.jsp; refs. 28, 29), and Reactome (http://www.reactome.org/ReactomeGWT/entrypoint.html; ref. 30). We then framed the biologic context of these genes signatures by mapping them to known molecular pathways [Ingenuity pathway analysis (IPA)]. For this study, gene expression magnitude and direction for network visualization was derived using the z-score from univariate SAM analysis in the external cohort with survival as the dependent variable.

All analyses were conducted using MATLAB (MathWorks Inc.), R (v. 2.11.1), SAS™ (v9.2, SAS), and IPA (v9.0, Ingenuity).

Results

Study, external, and validation cohorts

Twenty-five tumors from 25 patients with a median age of 71 years (range, 50–86), who had predominantly early-stage adenocarcinoma with lobectomy conducted were identified for the study cohort (Table 1). The median time to operation from PET acquisition was 27 days, and median tumor diameter (in the largest measured dimension) was 2.3 cm. The external cohort consisted of 63 patients with adenocarcinoma and a median age of 60 years. For the external cohort, 81% of patients were stage I–II with a median tumor diameter of 3.5 cm, follow-up of 42 months, and 24 (38%) deaths in the follow-up (Supplementary Data S1). The validation cohort consisted of 84 patients who had similar patient characteristics to the study cohort discounting gender (Table 1), SUV_{median} and SUV_{min}, for which significant differences existed among variables (Table 1). Median follow-up time in the validation cohort was 38 months, during which time, 21 (25%) patients died.

FDG uptake measurements

Blood glucose (mg/dL), injected dose (mCi), and time to scan (minutes) were similar between the study and validation cohorts except for time to scan, which was longer in the study cohort (Table 1). ROI segmentation and feature extraction was fully automated for all patients in the discovery cohort using RT_Image, but 9 of 84 patients (11%) in the validation group required manual override due to improper segmentation from the RT_Image algorithm.

Table 1. Characteristics of study and validation cohorts

	Study (N = 25)	Validation (N = 84)
Age, y	68 (63–72)	71 (64–77)
Male gender	18 (72)	38 (45)[d]
Ethnicity		
Caucasian	17 (60)	50 (60)
Asian	3 (12)	19 (22)
Other	5 (20)	1 (18)
Tumor diameter, cm	2.3 (1.7–2.9)	2.5 (1.9–3.8)
Procedure		
Wedge resection	1 (4)	12 (14)
Lobectomy	24 (96)	61 (72)
Other	0 (0)	11 (13)
Stage		
I–II	24 (92)	84 (100)
III–IV	2 (8)	0 (0)
Histology		
Adenocarcinoma	20 (80)	60 (71)
Squamous	4 (16)	20 (24)
Other	1 (4)	4 (5)
PET to resection time, d	27 (9–45)	28 (13–47)
Glucose level at PET, mg/dL	106 (100–108)[e]	100 (95–108)
Time to scan, min	60 (60–71)	60 (60–60)[d]
Injected dose, mCi	14.5 (12.9–15.8)	14.8 (13.5–16.4)
FDG uptake imaging features		
Intensity metrics		
SUV_{max}	3.2 (2.6–7.4)	5.9 (3.3–12.1)
SUV_{median}	1.8 (1.5–2.3)	2.6 (1.8–4.2)[d]
SUV_{mean}	1.9 (1.7–2.8)	2.9 (1.9–4.8)
$SUV_{75\%}$	3.4 (1.9–3.4)	3.2 (1.6–5.2)
$SUV_{90\%}$	2.5 (2.2–4.7)	4.3 (2.5–8.1)
SUV_{min}	1.4 (1.2–1.6)	1.8 (1.4–2.4)[d]
Distribution metrics		
$SUV_{kurtosis}$[a]	–0.06 (–0.53–0.61)	–0.14 (–0.60–0.51)
SUV_{skew}[a]	0.87 (0.66–1.2)	0.83 (0.61–1.1)
SUV_{sigma}	0.48 (0.27–1.3)	0.96 (0.47–2.2)
$SUV_{variance}$	0.23 (0.07–1.7)	0.92 (0.22–4.6)
Spatial metrics		
SUV_{MTV}, cm³	3.8 (2.0–13)	6.7 (3.5–25)
SUV_{area}, cm²	11.6 (4.8–41)	16.6 (8.1–59)
SUV_{points}[b]	67 (26–249)	97 (46–342)
SUV_{TGV},[c] cm³	13 (4.0–30)	22 (8.0–91)

NOTE: Continuous variables are shown with median and interquartile range and categorical variables with number and percentage.
[a]Kurtosis represents "peakedness" of FDG uptake, skew the deviation from a normal distribution, and sigma and variance the breadth of uptake distribution.
[b]Number of voxels used to generate MTV.
[c]Equivalent to the product of SUV_{mean} and SUV_{MTV}.
[d]$P < 0.05$ between study and validation cohorts for these variables.
[e]For 10 of 25 patients where data were available.

Table 2. Genes and metagenes associated with FDG uptake features in study cohort

Gene	Functional annotation	SUV-associated FDG uptake feature
BIRC2	Baculoviral IAP repeat containing 2	SUV_{mean}
FAP	Fibroblast activation protein, alpha	SUV_{mean}, SUV_{median}, SUV_{TGV}
FURIN	Paired basic amino acid cleaving enzyme	SUV_{mean}, $SUV_{75th\ percentile}$
LOC648470	Caspase 4, apoptosis-related cysteine peptidase	SUV_{mean}, SUV_{median}
LY6E	Lymphocyte antigen 6 complex, locus E	SUV_{skew}
MCM6	Minichromosome maintenance complex component 6	SUV_{skew}
RNF149	Ring finger protein 149	SUV_{mean}
OBFC1	Oligonucleotide-binding fold containing 1	SUV_{area}, SUV_{MTV}

Metagene[a]	Genes (*n*)	Functional annotation[b]	SUV-associated FDG uptake feature
Metagene 10	52	Focal and cell adhesion	SUV_{mean}, SUV_{median}, SUV_{TGV}
Metagene 18	36	Protein catabolism	SUV_{max}, $SUV_{variance}$
Metagene 26	18	Nucleic acid processing	SUV_{skew}
Metagene 30	19	Metalloproteinase genes, collagen	SUV_{mean}, SUV_{median}, SUV_{max}
Metagene 70	34	Targets of TP53, RB1	$SUV_{minimum}$
Metagene 78	19	Protein processing	SUV_{TGV}
Metagene 86	34	Embryogenesis, apoptosis	SUV_{max}, SUV_{TGV}
Metagene 100	25	Extracellular matrix, hypoxia and apoptosis	SUV_{max}, SUV_{TGV}

NOTE: FDR = 0 by SAM, per Patients and Methods.
[a]See Supplementary Data S2 for a full list of genes comprising each metagene.
[b]See Supplementary Data S3 and S4 for a full list of enrichment features associated with metagenes.

In the study cohort, median calculated SUV_{max} from RT_Image was 3.2 (range, 0.98–30), which agreed well with human observation by a certified nuclear medicine physician (A. Quon, $r = 0.91$). FDG uptake features between study and validation cohorts were reasonably similar in distribution but differed significantly for SUV_{median} and SUV_{min} (Table 1). SUV_{max} was highly correlated ($r > 0.8$) with mean, median, sigma, variance, total glycolytic volume, and percentile metrics, moderately correlated ($r > 0.6$) with minimum, area, volume and points metrics, and modestly correlated with skew and kurtosis features ($r = 0.48$ and 0.32, respectively).

Principal components analysis of FDG uptake features

The first three principal components explained 96% of the image feature variance for the study cohort and defined new FDG uptake features. The first principal component was dominated by traditional point estimates of FDG uptake features (SUV_{max}, SUV_{mean}, and SUV_{median}) and spatial metrics (SUV_{points}, SUV_{MTV}, and SUV_{area}). The second and third components were associated with $SUV_{kurtosis}$ and SUV_{skew}, measures of the shape of FDG uptake distribution, as well as SUV_{min}. These three principal components were added into a subsequent analysis with the initial 14 imaging features to examine their association with survival in the external cohort.

Gene expression and FDG uptake feature associations in the study cohort

In the study cohort, 37,798 assayed genes were filtered according to a 60% call rate (i.e., only those genes appearing in > 60% of samples were carried forward) to yield 8,238 present genes. After applying a variance filter described in the Patients and Methods, approximately half of these genes were included for further analysis. Eight of these 4,261 single genes were strongly associated with 7 different FDG uptake features by SAM analysis (Table 2). SUV_{mean} was significantly associated with 5 genes and SUV_{mean} and SUV_{skew} were the only FDG uptake features uniquely associated with single genes.

Fifty-six high-quality gene clusters (representing 2,300 individual genes, per Patients and Methods) were correlated to the FDG uptake features using SAM analysis. Eight of these metagenes consisting of 240 individual genes were significantly associated with 7 different FDG uptake features (FDR = 0), and SUV_{max} and SUV_{mean} features were enriched in extracellular matrix components in the study cohort (Table 2). Imaging features SUV_{skew}, SUV_{min}, and SUV_{TGV} were uniquely associated with metagenes enriched in protein and nucleic acid catabolism, as well as tumor suppressor pathways.

Predicted FDG uptake features and their association with survival

Predicted FDG uptake imaging features with an acceptable accuracy were carried forward to subsequent survival analysis (Table 3). All features passed this quality control except the third PCA (SUV_{PCA3}). Predicted $pSUV_{max}$, $pSUV_{mean}$, $pSUV_{min}$, $pSUV_{variance}$, and $pSUV_{PCA2}$ were significantly associated with survival in the external cohort (Table 4). A multivariate model of predicted FDG uptake features associated with survival identified $pSUV_{max}$, $pSUV_{variance}$, and $pSUV_{PCA2}$ as the top 3

Table 3. Accuracy of gene signatures that predict FDG uptake features in study cohort

Predicted FDG uptake feature	Accuracy[a]	Metagenes (n)	Genes (n)
$p\text{SUV}_{max}$	0.774	15	508
$p\text{SUV}_{mean}$	0.765	13	428
$p\text{SUV}_{median}$	0.748	13	428
$p\text{SUV}_{min}$	0.762	18	612
$p\text{SUV}_{90\%}$	0.765	16	552
$p\text{SUV}_{75\%}$	0.777	14	458
$p\text{SUV}_{sigma}$	0.765	16	555
$p\text{SUV}_{variance}$	0.804	12	387
$p\text{SUV}_{skew}$	0.784	14	516
$p\text{SUV}_{kurtosis}$	0.725	18	589
$p\text{SUV}_{area}$	0.866	11	300
$p\text{SUV}_{points}$	0.875	10	270
$p\text{SUV}_{MTV}$	0.871	10	270
$p\text{SUV}_{TGV}$	0.854	11	315
$p\text{SUV}_{PCA1}$	0.793	13	458
$p\text{SUV}_{PCA2}$	0.765	16	473

NOTE: Predicted features are denoted with a prefix "p" and are based on a linear combination of genes from the study cohort (see Patients and Methods).

[a]Accuracy defined as $1 - \sum_{k=1}^{25} |p\text{FDGfeature}_x - \text{FDGfeature}_x| / \Delta\text{range}$ (19).

prognostic FDG uptake features for predicting poor outcomes, with associated weights of 0.260, −0.281, and 0.148 respectively; we refer to this model as the multivariate-SUV model. Compared with the univariate FDG uptake features, the multivariate-SUV model yielded greatest prognostic value in the external cohort [HR, 5.87; confidence interval (CI), 2.59–13.8]. For single genes, 4 of 8 genes associated with FDG uptake from the study cohort were significantly associated with survival in the external data set (Table 4).

Validation of the prognostic FDG uptake features

We validated the significance of the predicted FDG uptake features that were associated with prognostic gene signatures on outcome in an additional 84 patient cohort with image data and survival data (Table 4). Both SUV_{max} (HR, 1.05; CI, 1.00–1.10) and the multivariate-SUV model (HR, 6.12; CI, 1.08–34.8) were significantly associated with survival by univariate CPH analysis and Kaplan–Meier plot (Fig. 2). The prognostic significance of SUV_{mean} ($P = 0.08$), SUV_{PCA2} ($P = 0.08$), $\text{SUV}_{variance}$ ($P = 0.16$), and SUV_{min} ($P = 0.62$) were not confirmed in the validation cohort, although the first 2 features maintained a strong trend with outcome ($P < 0.10$).

Incorporating clinical variables with prognostic FDG uptake features

In a univariate analysis, tumor size (cm) and stage (I–IV) were prognostically significant in both the external and vali-

dation cohorts (Supplementary Data S6). After adjusting for the clinical variables tumor size, stage, and age, $p\text{SUV}_{max}$ was found to be independently significant for predicting worse outcome in the external cohort (Supplementary Data S6). Adjusted point estimates for the HRs associated with SUV_{max} in the validation cohort, as well as the multivariate-SUV feature in the external and validation cohorts, were all greater than 1.0 but not statistically significant (Supplementary Data S6).

Gene network analysis

We further used network analysis and gene enrichment databases to inform us of important functional relationships between imaging features and gene expression for $p\text{SUV}_{max}$ and the multivariate-$p\text{SUV}$ model. $p\text{SUV}_{max}$, comprising 15 metagenes and 508 individual genes, was enriched in cell cycle (CDK2NA–p16) and acetylation (histone) pathways with network analysis showing a prominent NF-κB node (Supplementary Data S7). Of the 1,367 genes comprising the multivariate-$p\text{SUV}$ model, 484 were duplicated between features, leaving 883 unique genes to map for network analysis. Multiple important oncogenic pathways including cell proliferation (STAT1, PKA, FGF), cell cycle (CCNB, CCND, CEPBA), apoptosis (BAX, caspase, BIRC5), endocytosis (COP–Clathrin pathways), cell recognition (HLA-MHC), and oxidative phosphorylation (SLC25, cytochrome C, COX) were distinct nodes in this network (Supplementary Data S7).

Discussion

Aberrant cell signaling, proliferation, and immortality are well-known hallmarks of cancer (31). We show here that gene expression related to prognostic FDG uptake features was enriched in these canonical pathways. Emerging hallmarks of cancer, including cell bioenergetics, inflammation, and immune evasion, may also play an important role in defining FDG uptake as a global marker of poor prognosis in patients with resected NSCLCs according to our analysis. Finally, increasing SUV_{max} is well established to be associated with poor patient outcome (3–5), and our analysis suggests that NF-κB signaling is a key molecular correlate for this imaging biomarker. This is a provocative finding, as NF-κB signaling is activated downstream by lactate production from glycolysis and—like FDG uptake—is increased in inflammatory and malignant diseases (32).

By using a computational design for this study, we examined multiple prognostic FDG uptake imaging features with genome-wide expression from NSCLC tumors. After accounting for multiple comparisons with FDR analysis ($q < 0.05$), we show that novel FDG uptake features were associated with distinct genes and gene signatures, less related (i.e., correlated) features were associated with different genes and gene signatures, and in combination features provided a more prognostic model than any one feature alone.

One previous study has investigated gene expression across varying degrees of FDG uptake in breast cancer, as defined by SUV_{max}, and glycolytic genes were remarkably absent from the most highly significant associations—as was the case in our study (Supplementary Data S8; ref. 33). A follow-up to that study

Table 4. Prognostic significance of genes, metagenes, and associated FDG uptake features in external and validation cohorts

		Univariate survival analysis		
Gene	Function of gene	HR (95% CI); external cohort	SUV-associated FDG uptake feature	HR (95% CI) validation Cohort
FAP	Fibroblast proliferation and activation	1.45 (1.00–2.09)	SUV_{mean}	1.13 (0.99–1.30)
			SUV_{median}	1.15 (0.98–1.34)
			SUV_{TGV}	1.00 (1.00–1.00)[e]
RNF149	Unknown	2.20 (1.42–3.39)	SUV_{mean}	1.13 (0.99–1.30)
LY6E	Immune recognition and cell trafficking	1.46 (1.04–2.05)	SUV_{skew}	1.69 (0.69–4.11)
MCM6	Genome replication/cell proliferation	1.49 (1.06–2.11)	SUV_{skew}	1.69 (0.69–4.11)
Predicted FDG uptake feature	**Functional enrichment[a,b]**	**HR (95% CI); external cohort**	**SUV-associated FDG uptake feature**	**HR (95% CI) validation Cohort**
$pSUV_{max}$[c]	Cell cycle and extracellular matrix (ECM)	1.56 (1.07–2.28)	SUV_{max}	1.05 (1.00–1.10)
$pSUV_{mean}$[c]	Cell cycle and immune response	1.55 (1.03–2.33)	SUV_{mean}	1.13 (0.99–1.30)
$pSUV_{variance}$[c]	Cell cycle and ECM	0.69 (0.49–0.97)	$SUV_{variance}$	1.06 (0.99–1.41)
$pSUV_{min}$[c]	Cell signaling and ECM	1.60 (1.03–2.46)	SUV_{min}	1.12 (0.73–1.78)
$pSUV_{PCA2}$[c]	Antigen presentation and processing	1.49 (1.02–2.19)	SUV_{PCA2}	1.24 (0.97–1.59)
Multivariate-$pSUV$[c,d]	Cell/antigen processing, immune response, ECM	5.87 (2.59–13.8)	Multivariate-SUV[d]	6.12 (1.08–34.8)

NOTE: For overall survival, external cohort ($n = 63$) and validation cohort ($n = 84$). See Supplementary Data S6 for analyses with clinical variables and imaging features.
[a]See Supplementary Data S2 for a full list of genes associated with metagenes.
[b]See Supplementary Data S3 and S4 for enrichment analysis of gene lists using DAVID and GSEA bioinformatics tools.
[c]p denotes predicted features defined by gene expression and examined in the external cohort.
[d]Multivariate expression coefficients for SUV_{max}, $SUV_{variance}$, and SUV_{PCA2} were 0.260, −0.281, and 0.148, respectively.
[e]$P = 0.001$.

focusing on cell bioenergetics found that glycolytic pathways are upregulated in the context of other major tumor pathways but are not the most highly enriched pathways (34). Interestingly, this follow-up study focused on another important driver of oncogenesis, c-MYC, and related it to FDG uptake. In contrast, our study's prognostic multivariate-SUV feature was associated with other major drivers of oncogenesis, although we also found that MYC-related pathways were enriched during ontology analysis (Supplementary Data S3 and S4).

Models such as these may deepen the use, and our understanding, of FDG uptake as a biomarker and may provide additional insight at the genomic level for a tumor phenotype defined by heterogeneous FDG uptake at the imaging level. The Warburg effect was initially described more than 80 years ago and postulates that tumors undergo glycolysis preferentially despite adequate intracellular oxygen tension (35, 36). Although Warburg believed that this

was a result of mitochondrial dysfunction, we now know that tumor glycolysis can proceed with functional cellular mitochondria and in fact may be an adaptive response for tumor survival (10, 11, 37). Furthermore, studies have recently linked glycolysis in cancer to more widespread dysregulation of cell bioenergetics (38–40), suggesting that FDG uptake may be a surrogate for more than glycolysis alone and perhaps a lens through which one can view global tumor bioenergetics.

This study has limitations. To identify the prognostic significance of FDG features and their associated gene signatures, the ideal cohort would typically consist of hundreds of patients with: (i) genomic profiling of their resected tumor, (ii) PET imaging of the tumor before resection, and (iii) long-term follow-up. Because such large cohorts are not yet commonly available, we present and implemented a novel technique that integrates the three data types (namely,
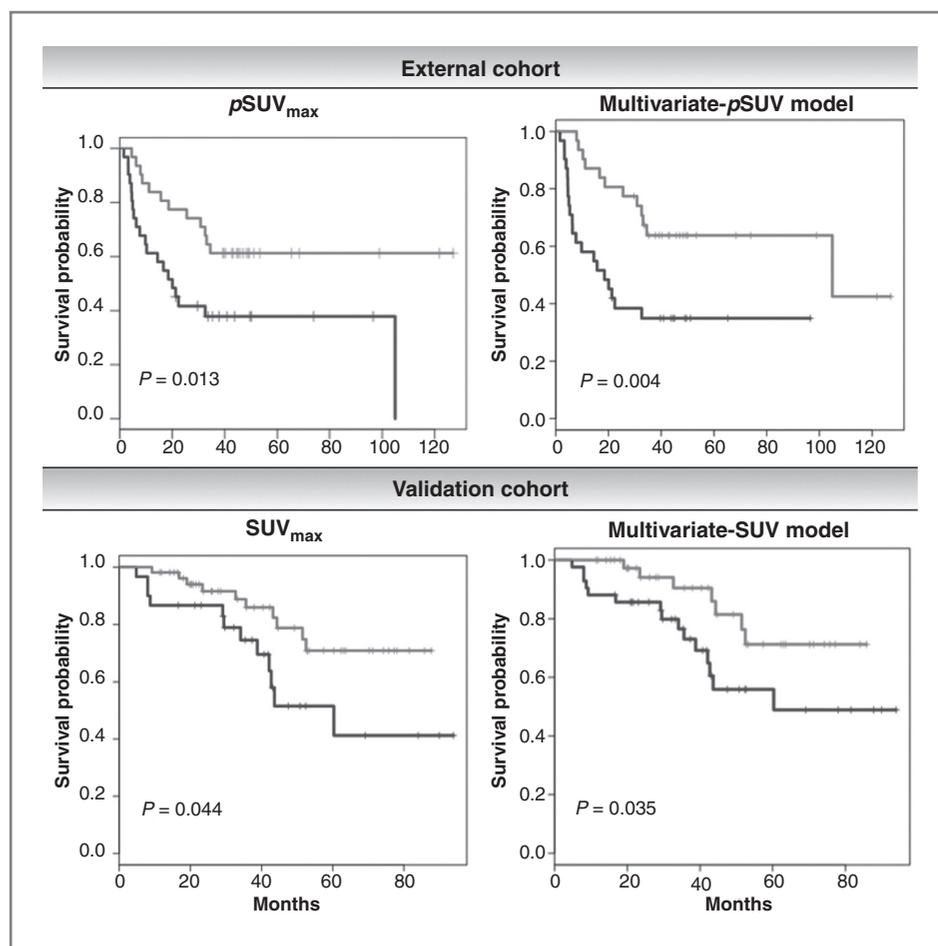
Figure 2. Overall survival for prognostically significant FDG uptake features dichotomized at the median value. Survival analysis showed that SUV_{max} and the multivariate-SUV model were prognostically significant in external and validation cohorts, respectively. In the external cohort, the predicted image features (denoted by the prefix "p") were assessed. Worse versus better survival is illustrated by the dark gray versus gray curves. The y-axis represents percentage alive and the x-axis is months to event. Note that the x-axis is different for the 2 cohorts, as duration of follow-up time was unique for each cohort. Supplementary Data S5 provides additional plots for prognostic single genes associated with FDG uptake.

gene expression, imaging, and survival data) from three different cohorts.

We did not apply a correction of PET-FDG signal that may sometimes be required for tumors that approach the resolution of the PET scanner ($\sim$1.5–2.0 cm)—known as partial volume effect correction—to our data (41, 42). While some studies have shown that this can have a significant effect on traditionally used metrics of uptake, such as SUV_{max} and SUV_{mean}, (43), the effect of correcting for more novel features, such as SUV_{MTV} and SUV_{skew}, is unresolved to date (44). In addition to the above intrascan variation, interscan variation between PET scanners exists, can add to imprecision for feature quantification, and should be accounted for in future multicenter studies (45).

Although our sample was predominantly adenocarcinoma, there was some heterogeneity in histology, which is well known to affect both FDG uptake and gene expression (46, 47). We may not have exploited the full gamut of prognostic imaging features we derived using RT_Image as we were interested in examining only those FDG uptake features that were associated with prognostic gene signatures. Finally, the added significance of prognostic imaging features and their associated gene profiles compared with traditional clinical variables of prognosis was marginal, possibly due to the sample size and heterogeneity of the cohorts examined. Yet, our results indicate

that larger studies are warranted to evaluate the prognostic significance of a broader characterization of FDG uptake features and to assess the relationship of FDG uptake to molecular processes beyond glycolysis.

Conclusion

Using gene leveraging techniques can harness the power of the public domain for expediting studies of radiogenomic biomarkers. A computational approach to understanding gene expression correlates of aggressive NSCLC as defined by prognostic ^{18}F-FDG uptake features may offer new insights into tumor biology. Our methods require further study in other human cancers and larger, homogeneous cohorts of patients with NSCLC with standardized gene expression, imaging, and clinical data.

Disclosure of Potential Conflicts of Interest

No potential conflicts of interest were disclosed.

Authors' Contributions

Conception and design: V.S. Nair, O. Gevaert, S. Napel, E.E. Graves, A. Quon, D.L. Rubin, S.K. Plevritis
Development of methodology: V.S. Nair, O. Gevaert, S. Napel, E.E. Graves, J.B. Shrager, A. Quon, S.K. Plevritis
Acquisition of data (provided animals, acquired and managed patients, provided facilities, etc.): V.S. Nair, G. Davidzon, C.D. Hoang, J.B. Shrager, A. Quon, S.K. Plevritis
Analysis and interpretation of data (e.g., statistical analysis, biostatistics, computational analysis): V.S. Nair, O. Gevaert, G. Davidzon, A. Quon, S.K. Plevritis

References

1. Jemal A, Siegel R, Xu J, Ward E. Cancer statistics, 2010. CA Cancer J Clin 2010;60:277–300.
2. Pignon JP, Tribodet H, Scagliotti GV, Douillard JY, Shepherd FA, Stephens RJ, et al. Lung adjuvant cisplatin evaluation: a pooled analysis by the LACE Collaborative Group. J Clin Oncol 2008; 26:3552–9.
3. Berghmans T, Dusart M, Paesmans M, Hossein-Foucher C, Buvat I, Castaigne C, et al. Primary tumor standardized uptake value (SUVmax) measured on fluorodeoxyglucose positron emission tomography (FDG-PET) is of prognostic value for survival in non-small cell lung cancer (NSCLC): a systematic review and meta-analysis (MA) by the European Lung Cancer Working Party for the IASLC Lung Cancer Staging Project. J Thorac Oncol 2008;3:6–12.
4. Nair VS, Barnett PG, Ananth L, Gould MK. PET scan 18F-fluorodeoxyglucose uptake and prognosis in patients with resected clinical stage IA non-small cell lung cancer. Chest 2010;137:1150–6.
5. Paesmans M, Berghmans T, Dusart M, Garcia C, Hossein-Foucher C, Lafitte JJ, et al. Primary tumor standardized uptake value measured on fluorodeoxyglucose positron emission tomography is of prognostic value for survival in non-small cell lung cancer: update of a systematic review and meta-analysis by the European Lung Cancer Working Party for the International Association for the Study of Lung Cancer Staging Project. J Thorac Oncol 2010;5: 612–9.
6. Gould MK, Kuschner WG, Rydzak CE, Maclean CC, Demas AN, Shigemitsu H, et al. Test performance of positron emission tomography and computed tomography for mediastinal staging in patients with non-small-cell lung cancer: a meta-analysis. Ann Intern Med 2003; 139:879–92.
7. Gould MK, Sanders GD, Barnett PG, Rydzak CE, Maclean CC, McClellan MB, et al. Cost-effectiveness of alternative management strategies for patients with solitary pulmonary nodules. Ann Intern Med 2003; 138:724–35.
8. Gambhir SS, Shepherd JE, Shah BD, Hart E, Hoh CK, Valk PE, et al. Analytical decision model for the cost-effective management of solitary pulmonary nodules. J Clin Oncol 1998;16:2113–25.
9. van Tinteren H, Hoekstra OS, Smit EF, van den Bergh JH, Schreurs AJ, Stallaert RA, et al. Effectiveness of positron emission tomography in the preoperative assessment of patients with suspected non-small-cell lung cancer: the PLUS multicentre randomised trial. Lancet 2002;359:1388–93.
10. Mathupala SP, Ko YH, Pedersen PL. Hexokinase-2 bound to mitochondria: cancer's stygian link to the "Warburg Effect" and a pivotal target for effective therapy. Semin Cancer Biol 2009;19:17–24.
11. Frezza C, Gottlieb E. Mitochondria in cancer: not just innocent bystanders. Semin Cancer Biol 2009;19:4–11.
12. Shanmugam M, McBrayer SK, Rosen ST. Targeting the Warburg effect in hematological malignancies: from PET to therapy. Curr Opin Oncol 2009;21:531–6.
13. Semenza GL. Hypoxia and cancer. Cancer Metastasis Rev 2007; 26:223–4.
14. Koppenol WH, Bounds PL, Dang CV. Otto Warburg's contributions to current concepts of cancer metabolism. Nat Rev Cancer 2011;11: 325–37.
15. Christofk HR, Vander Heiden MG, Harris MH, Ramanathan A, Gerszten RE, Wei R, et al. The M2 splice isoform of pyruvate kinase is important for cancer metabolism and tumour growth. Nature 2008;452:230–3.
16. Christofk HR, Vander Heiden MG, Wu N, Asara JM, Cantley LC. Pyruvate kinase M2 is a phosphotyrosine-binding protein. Nature 2008;452:181–6.
17. Vander Heiden MG, Locasale JW, Swanson KD, Sharfi H, Heffron GJ, Amador-Noguez D, et al. Evidence for an alternative glycolytic pathway in rapidly proliferating cells. Science 2010;329:1492–9.
18. Yang W, Xia Y, Ji H, Zheng Y, Liang J, Huang W, et al. Nuclear PKM2 regulates beta-catenin transactivation upon EGFR activation. Nature 2011;480:118–22.
19. Gevaert O, Xu J, Hoang C, Leung A, Xu Y, Quon A, et al. Identification of prognostic imaging biomarkers for non-small cell lung cancer by leveraging public gene expression microarray data. Radiology. 2012.
20. Lee ES, Son DS, Kim SH, Lee J, Jo J, Han J, et al. Prediction of recurrence-free survival in postoperative non-small cell lung cancer patients by using an integrated model of clinical information and gene expression. Clin Cancer Res 2008;14:7397–404.
21. Graves EE, Quon A, Loo BW Jr. RT_Image: an open-source tool for investigating PET in radiation oncology. Technol Cancer Res Treat 2007;6:111–21.
22. La TH, Filion EJ, Turnbull BB, Chu JN, Lee P, Nguyen K, et al. Metabolic tumor volume predicts for recurrence and death in head-and-neck cancer. Int J Radiat Oncol Biol Phys 2009;74:1335–41.
23. Tibshirani R, Hastie T, Narasimhan B, Chu G. Diagnosis of multiple cancer types by shrunken centroids of gene expression. Proc Natl Acad Sci U S A 2002;99:6567–72.
24. Bild AH, Yao G, Chang JT, Wang Q, Potti A, Chasse D, et al. Oncogenic pathway signatures in human cancers as a guide to targeted therapies. Nature 2006;439:353–7.
25. Tibshirani R. The lasso method for variable selection in the Cox model. Stat Med 1997;16:385–95.
26. Benjamini Y, Hochberg Y. Controlling the false discovery rate: a practical and powerful approach to multiple testing. J R Stat Soc Ser B 1995;57:289–300.
27. Huang da W, Sherman BT, Lempicki RA. Systematic and integrative analysis of large gene lists using DAVID bioinformatics resources. Nat Protoc 2009;4:44–57.
28. Culhane AC, Schwarzl T, Sultana R, Picard KC, Picard SC, Lu TH, et al. GeneSigDB–a curated database of gene expression signatures. Nucleic Acids Res 2010;38(Database issue):D716–25.

29. Huang da W, Sherman BT, Lempicki RA. Bioinformatics enrichment tools: paths toward the comprehensive functional analysis of large gene lists. Nucleic Acids Res 2009;37:1–13.

30. Croft D, O'Kelly G, Wu G, Haw R, Gillespie M, Matthews L, et al. Reactome: a database of reactions, pathways and biological processes. Nucleic Acids Res 2011;39(Database issue):D691–7.

31. Hanahan D, Weinberg RA. Hallmarks of cancer: the next generation. Cell 2011;144:646–74.

32. Hirschhaeuser F, Sattler UG, Mueller-Klieser W. Lactate: a metabolic key player in cancer. Cancer Res 2011;71:6921–5.

33. Osborne JR, Port E, Gonen M, Doane A, Yeung H, Gerald W, et al. 18F-FDG PET of locally invasive breast cancer and association of estrogen receptor status with standardized uptake value: microarray and immunohistochemical analysis. J Nucl Med 2010;51:543–50.

34. Palaskas NJ, Larson SM, Schultz N, Komisopoulou E, Wong J, Rohle D, et al. 18F-fluorodeoxy-glucose positron emission tomography (18FDG-PET) marks MYC-overexpressing human basal-like breast cancers. Cancer Res 2011;71:5164–74.

35. Warburg O. On respiratory impairment in cancer cells. Science 1956;124:269–70.

36. Warburg O. On the origin of cancer cells. Science 1956;123:309–14.

37. Robey RB, Hay N. Is Akt the "Warburg kinase"?-Akt-energy metabolism interactions and oncogenesis. Semin Cancer Biol 2009;19:25–31.

38. Dang CV. Enigmatic MYC conducts an unfolding systems biology symphony. Genes Cancer 2010;1:526–31.

39. Dang CV. Glutaminolysis: supplying carbon or nitrogen or both for cancer cells? Cell Cycle 2010;9:3884–6.

40. Dang CV. Rethinking the Warburg effect with Myc micromanaging glutamine metabolism. Cancer Res 2010;70:859–62.

41. Boellaard R, Krak NC, Hoekstra OS, Lammertsma AA. Effects of noise, image resolution, and ROI definition on the accuracy of standard uptake values: a simulation study. J Nucl Med 2004;45:1519–27.

42. Soret M, Bacharach SL, Buvat I. Partial-volume effect in PET tumor imaging. J Nucl Med 2007;48:932–45.

43. Vesselle H, Freeman JD, Wiens L, Stern J, Nguyen HQ, Hawes SE, et al. Fluorodeoxyglucose uptake of primary non-small cell lung cancer at positron emission tomography: new contrary data on prognostic role. Clin Cancer Res 2007;13:3255–63.

44. Tylski P, Stute S, Grotus N, Doyeux K, Hapdey S, Gardin I, et al. Comparative assessment of methods for estimating tumor volume and standardized uptake value in (18)F-FDG PET. J Nucl Med 2010;51:268–76.

45. Velasquez LM, Boellaard R, Kollia G, Hayes W, Hoekstra OS, Lammertsma AA, et al. Repeatability of 18F-FDG PET in a multicenter phase I study of patients with advanced gastrointestinal malignancies. J Nucl Med 2009;50:1646–54.

46. Bhattacharjee A, Richards WG, Staunton J, Li C, Monti S, Vasa P, et al. Classification of human lung carcinomas by mRNA expression profiling reveals distinct adenocarcinoma subclasses. Proc Natl Acad Sci U S A 2001;98:13790–5.

47. Casali C, Cucca M, Rossi G, Barbieri F, Iacuzio L, Bagni B, et al. The variation of prognostic significance of maximum standardized uptake value of [18F]-fluoro-2-deoxy-glucose positron emission tomography in different histological subtypes and pathological stages of surgically resected non-small cell lung carcinoma. Lung Cancer 2010;69:187–93.

Correction: Prognostic PET ^{18}F-FDG Uptake Imaging Features Are Associated with Major Oncogenomic Alterations in Patients with Resected Non–Small Cell Lung Cancer

In this article (Cancer Res 2012;72:3725–34), which was published in the August 1, 2012 issue of *Cancer Research* (1), the following typographical errors appeared in the Patients and Methods section on page 3727:

1) Duplicate paragraphs appeared under the headings comparison of study and validation cohorts and statistical analysis.
2) The phrase "significance-predicated" under the heading predicted FDG uptake features and their association with overall survival should have read "significance for predicted."

In addition, Table 1 contained typographical errors as follows: The 1st column under the Stage header should read "Stage I-II 24 (96) and "Stage III-IV 1 (4)" rather than "Stage I-II 24 (92)" and "Stage III-IV 2 (8)." The second column under the Ethnicity-Other header should read "15 (18)" rather than "1 (18)."
The corrected version of Table 1 is provided below.

Table 1. Characteristics of study and validation cohorts

	Study (*N* = 25)	Validation (*N* = 84)
Age, y	68 (63–72)	71 (64–77)
Male gender	18 (72)	38 (45)[d]
Ethnicity		
Caucasian	17 (60)	50 (60)
Asian	3 (12)	19 (22)
Other	5 (20)	15 (18)
Tumor diameter, cm	2.3 (1.7–2.9)	2.5 (1.9–3.8)
Procedure		
Wedge resection	1 (4)	12 (14)
Lobectomy	24 (96)	61 (72)
Other	0 (0)	11 (13)
Stage		
I–II	24 (96)	84 (100)
III–IV	1 (4)	0 (0)
Histology		
Adenocarcinoma	20 (80)	60 (71)
Squamous	4 (16)	20 (24)
Other	1 (4)	4 (5)
PET to resection time, d	27 (9–45)	28 (13–47)
Glucose level at PET, mg/dL	106 (100–108)[e]	100 (95–108)
Time to scan, min	60 (60–71)	60 (60–60)[d]
Injected dose, mCi	14.5 (12.9–15.8)	14.8 (13.5–16.4)

(Continued on the following page)

Table 1. Characteristics of study and validation cohorts (Cont'd)

	Study (N = 25)	Validation (N = 84)
FDG uptake imaging features		
Intensity metrics		
SUV_{max}	3.2 (2.6–7.4)	5.9 (3.3–12.1)
SUV_{median}	1.8 (1.5–2.3)	2.6 (1.8–4.2)[d]
SUV_{mean}	1.9 (1.7–2.8)	2.9 (1.9–4.8)
$SUV_{75\%}$	3.4 (1.9–3.4)	3.2 (1.6–5.2)
$SUV_{90\%}$	2.5 (2.2–4.7)	4.3 (2.5–8.1)
SUV_{min}	1.4 (1.2–1.6)	1.8 (1.4–2.4)[d]
Distribution metrics		
$SUV_{kurtosis}$[a]	−0.06 (−0.53–0.61)	−0.14 (−0.60–0.51)
SUV_{skew}[a]	0.87 (0.66–1.2)	0.83 (0.61–1.1)
SUV_{sigma}	0.48 (0.27–1.3)	0.96 (0.47–2.2)
$SUV_{variance}$	0.23 (0.07–1.7)	0.92 (0.22–4.6)
Spatial metrics		
SUV_{MTV}, cm^3	3.8 (2.0–13)	6.7 (3.5–25)
SUV_{area}, cm^2	11.6 (4.8–41)	16.6 (8.1–59)
SUV_{points}[b]	67 (26–249)	97 (46–342)
SUV_{TGV},[c] cm^3	13 (4.0–30)	22 (8.0–91)

NOTE: Continuous variables are shown with median and interquartile range and categorical variables with number and percentage.
[a]Kurtosis represents "peakedness" of FDG uptake, skew the deviation from a normal distribution, and sigma and variance the breadth of uptake distribution.
[b]Number of voxels used to generate MTV.
[c]Equivalent to the product of SUV_{mean} and SUV_{MTV}.
[d]$P < 0.05$ between study and validation cohorts for these variables.
[e]For 10 of 25 patients where data were available.

Reference

1. Nair VS, Gevaert O, Davidzon G, Napel S, Graves EE, Hoang CD, et al. Prognostic PET ^{18}F-FDG uptake imaging features are associated with major oncogenomic alterations in patients with resected non–small cell lung cancer. Cancer Res 2012;72:3725–34.

Cancer Research

The Journal of Cancer Research (1916–1930) | The American Journal of Cancer (1931–1940)

AACR American Association for Cancer Research

Prognostic PET ^{18}F-FDG Uptake Imaging Features Are Associated with Major Oncogenomic Alterations in Patients with Resected Non –Small Cell Lung Cancer

Viswam S. Nair, Olivier Gevaert, Guido Davidzon, et al.

Updated version	Access the most recent version of this article at: doi:10.1158/0008-5472.CAN-11-3943
Supplementary Material	Access the most recent supplemental material at: http://cancerres.aacrjournals.org/content/suppl/2012/06/18/0008-5472.CAN-11-3943.DC1

Cited articles	This article cites 46 articles, 16 of which you can access for free at: http://cancerres.aacrjournals.org/content/72/15/3725.full#ref-list-1
Citing articles	This article has been cited by 3 HighWire-hosted articles. Access the articles at: http://cancerres.aacrjournals.org/content/72/15/3725.full#related-urls

E-mail alerts	Sign up to receive free email-alerts related to this article or journal.
Reprints and Subscriptions	To order reprints of this article or to subscribe to the journal, contact the AACR Publications Department at pubs@aacr.org.
Permissions	To request permission to re-use all or part of this article, use this link http://cancerres.aacrjournals.org/content/72/15/3725. Click on "Request Permissions" which will take you to the Copyright Clearance Center's (CCC) Rightslink site.